

Investigating merging galaxies by using Pan-STARRS images[★]

Yi-Fan Lin¹, Po-Chieh Yu¹, Jen-Chao Huang¹, Chorng-Yuan Hwang¹, Wen-Ping Chen^{1,2},
Nick Kaiser³, Nigel Metcalfe⁴, and Christopher Waters³

¹ Graduate Institute of Astronomy, No. 300, Zhongda Rd., Zhongli Dist., Taoyuan City 32001, Taiwan
e-mail: pcyu@astro.ncu.edu.tw

² Department of Physics, No. 300, Zhongda Rd., Zhongli Dist., Taoyuan City 32001, Taiwan

³ Institute for Astronomy, University of Hawaii, 2680 Woodlawn Drive, Honolulu, HI 96822-1839, USA

⁴ Department of Physics, Durham University, South Road, Durham, DH1 3LE, UK

Received 29 March 2016 / Accepted 15 December 2016

ABSTRACT

Aims. We studied the r' -, z' -, and y' -band images of merging galaxies from the observations of the Panoramic Survey Telescope & Rapid Response System (Pan-STARRS). The merging galaxies were selected from our merging catalog that was created by checking the images of the Red-Sequence Cluster Survey 2 from the observations of the Canada France Hawaii Telescope.

Methods. By using the homomorphic-aperture, we determined the photometric results of these merging systems. To obtain accurate photometry, we calibrated the Pan-STARRS r' -, z' -, and y' -band data to match the results of Sloan Digital Sky Survey Data Release 9. We also investigated the stellar masses of the merging galaxies by comparing the Wide-field Infrared Survey Explorer 3.4 μm emission with the calibrated y' -band data.

Results. We present a catalog of the r' -, z' -, and y' -band photometric results for 4698 merging galaxies. For extended sources, our results suggest that the homomorphic-aperture method can obtain more reasonable results than the Desktop Virtual Observatory photometry. We derived new relations between the Pan-STARRS y' -band luminosities and the stellar masses of the merging galaxies. Our results show that the stellar masses of the merging galaxies range from 10^8 to $10^{13} M_{\odot}$; some of the dry mergers could be as massive as $10^{13} M_{\odot}$.

Key words. galaxies: general – galaxies: interactions – galaxies: irregular

1. Introduction

Merging galaxies play a crucial role in the evolution of galaxies. One of the most favorable models in galaxy evolution describes massive galaxies forming through major mergers, that is, the Λ CDM model (Cole et al. 2000). A merging system arising from two gas-poor galaxies is called a dry merger. By contrast, a merger system arising from two gas-rich galaxies is called a wet merger. Wet mergers usually ignite additional star formation (Nikolic et al. 2004; Lin et al. 2007), while dry mergers are suggested to involve in the stellar mass growth of massive galaxies (van Dokkum 2005; Lin et al. 2008). To unveil the process of galaxy formation and evolution, it is important to estimate the stellar mass of different types of mergers at high redshifts.

Galaxies transform their appearance during galaxy merging. Merging galaxies consist of unusual structures, such as bridges or tails, which are caused by a tidal force between galaxies (Toomre & Toomre 1972). Thus, the disturbed morphology of merging galaxies is a clear indication of merging systems. Because the morphology of merging galaxies varies, no reliable method can recognize merging galaxies automatically. Using visual inspection, several studies have searched for merging systems or close pairs such as the Galaxy Zoo project (van Dokkum 2005; Ellison et al. 2008; Darg et al. 2010; Sheen et al. 2012). However, adapting visual methods requires abundant manpower and is highly time-consuming; an effective method of identifying

merging galaxies automatically is in demand. Hwang & Chang (2009) developed an algorithm to separate normal and disturbed galaxies. They inspected the results derived from the algorithm with the naked eye before designating the merging galaxies and identified 15 147 merging galaxies from the Red-Sequence Cluster Survey 2 data (RCS2; Yee et al. 2007; Gilbank et al. 2011).

Numerous studies have determined the stellar mass of galaxies by using near-infrared observations (Bundy et al. 2005; Davoodi et al. 2006) or spectral synthesis fitting to optical spectra (Kauffmann et al. 2003; Tremonti et al. 2004). Generally, the mass of a galaxy is in an approximate range from 10^9 to $10^{12} M_{\odot}$. Although near-infrared observations are often used to estimate the stellar mass, they are more complex and difficult to use than optical observations. Also, with poor resolution, there might be some contamination from neighboring stars or galaxies. By contrast, optical observations are excessively affected by dust. Regarding the aforementioned conditions, employing an appropriate optical wavelength without significant dust extinction is highly useful in estimating the stellar mass.

The optical y' -band observations can effectively pass dust extinction. The center wavelength of the y' band is 10 000 Å; the wavelength of the y' -band is between the optical wavelength and the near-infrared wavelength. Furthermore, y' -band observations can be employed to study high redshift quasars and galaxies (Choi et al. 2012). Therefore, these observations might be a suitable tool for investigating stellar mass and galaxy evolution.

The first y' -band sky survey was conducted using the Panoramic Survey Telescope and Rapid Response System

[★] The catalog is only available at the CDS via anonymous ftp to cdsarc.u-strasbg.fr (130.79.128.5) or via <http://cdsarc.u-strasbg.fr/viz-bin/qcat?J/A+A/600/A28>

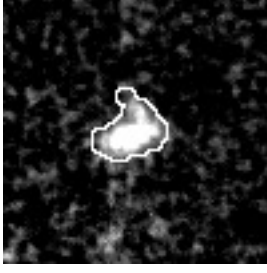


Fig. 1. Example of using homomorphic-aperture method.

(Pan-STARRS; Hodapp et al. 2004). The prototype of the Pan-STARRS, called Pan-STARRS1 (PS1), is a 1.8-m telescope located on Mount Halekala in Hawaii with a field of view of 3.3° . In this study, we used the y' -band images of Pan-STARRS to investigate the stellar mass of merging galaxies selected by Hwang & Chang (2009). We present our data reduction in Sect. 2 to describe our photometric process. In Sect. 3, we provide the stellar mass estimation of merging galaxies and the role of stellar mass in galaxy evolution in Sect. 4. We assume that the Hubble parameter $H_0 = 70 \text{ km s}^{-1} \text{ Mpc}^{-1}$, $\Omega_m = 0.3$, and $\Lambda_0 = 0.7$ throughout this paper.

2. Data reduction and analysis

We used the stack images (data release Version 3) of the Pan-STARRS 3 π survey to measure the combined r' -, z' -, and y' -band photometry of both components of a merging system. To obtain accurate photometric results, we used the homomorphic-aperture method to measure these merging galaxies (see also Huang & Hwang 2017). We first created clean images by producing mask images and subtracting the background. We then generated a binary image by applying a threshold to the clean images; in the binary image, a pixel would have a value equal to 1 (0) if the corresponding pixel in the clean image was higher (lower) than the local threshold. The threshold was determined empirically depending on the quality of the images. A low threshold may detect more faint signals, but might be contaminated by more noise. We used 4σ (the standard deviation of the background) as our threshold for the Pan-STARRS y' -band images after testing sources with known fluxes. A group of connected pixels that had a value equal to 1 in the binary image was considered as a source object. We employed the shape of the source object to create a homomorphic aperture for the source by dilating the source shape using the DILATION image operation, which extends the size of the object boundary by one pixel (Heijmans & Ronse 1990). Two dilations on the source objects were applied to obtain the homomorphic apertures (see Fig. 1 for an example).

2.1. Calibration with the SDSS

The zeropoints of PS1 stack images had been scaled to 25. To obtain accurate photometric results for the merging galaxies, stars from the Sloan Digital Sky Survey (SDSS; York et al. 2000) were employed to perform the calibration. The magnitude data of the stars were derived from the SDSS DR9 (Ahn et al. 2012) archive. We set the following criteria when selecting the calibrating stars: (1) the stars must be within a $3'$ radius of our targets; (2) the r' -band and z' -band magnitudes of the stars must be between 15 and 22.

Because no y' -band observation is available in the SDSS, the translation equation and parameters provided by Tonry et al. (2012) were used to obtain the y' -band magnitudes of the stars. Tonry et al. (2012) derived a relation between the z' -band of the SDSS and the y' -band of the PS1 for stellar objects. We could thus obtain the expected y' -band magnitudes of the calibrating stars from the SDSS z' -band magnitudes. However, only the stars with $g' - r' > 0.3$ can suitably fit in their relation (Fig. 6 in Tonry et al. 2012). Thus, only the stars with $g' - r' > 0.3$ from the SDSS were employed to perform the magnitude translation with the quadratic conversion formula:

$$y = A_0 + A_1x + A_2x^2, \quad (1)$$

where x refers to the color of $g' - r'$ in the SDSS; y is $y_{\text{PS1}} - z_{\text{SDSS}}$; A_0 is 0.031; A_1 is -0.106 ; and A_2 is 0.011 (Tonry et al. 2012). Because the limiting magnitude of the PS1 y' -band observations is approximately 20, we retained only the stars with derived y' -band magnitudes brighter than 20 for the calibration. In addition, to achieve accurate calibrations, only merging galaxies that had more than four calibrating stars were considered. We also used the same homomorphic-aperture method and set the same 4σ threshold on the calibrating stars for consistency in estimating the magnitudes.

We then compared the results of the stars between the PS1 and the SDSS. We estimated the difference of each star between the PS1 and SDSS in each band:

$$\text{difference} = \text{PS1} - \text{SDSS}. \quad (2)$$

After obtaining the difference of the stars, we calculated the mean difference of the calibrating stars of the merging galaxy. We then compared the individual difference with the mean difference:

$$\text{Diff1} = |\text{difference} - \text{mean}(\text{difference})|. \quad (3)$$

We empirically determined that if the *Diff1* value of a star was less than 1, it was a suitable star to be used in the fitting process; otherwise, we excluded the stars of which the *Diff1* value was greater than 1, which indicated that there was substantial difference between the PS1 and the SDSS observations. After excluding the unsuitable stars, we derived the mean difference again from the available stars. The mean difference (MD) was regarded as the calibrating difference between the PS1 and the SDSS,

$$\text{SDSS} = (\text{PS1} - \text{MD}). \quad (4)$$

We used the calibrating difference to calibrate our merging galaxies. Using the calibration process, the composite PS1 magnitudes of the merging galaxies were calibrated to the SDSS ones.

In total, we obtained calibrated photometry of 4698 merging galaxies, and their merged colors are shown in Fig. 2. The calibrated photometric results of the first 20 merging galaxies of the catalog are listed in Table 1. The complete catalog is available at the CDS and contains the following information. Column 1 gives the ID number of the source, Cols. 2 and 3 list the coordinates in degrees (J2000), Cols. 4, 6 and 8 represent r' -, z' -, and y' -band magnitudes after calibration with SDSS data, and Cols. 5, 7, and 9 give photometric uncertainties of r' -, z' -, and y' -band data.

Table 1. Composite photometric results for 20 merging galaxies.

ID	RA	Dec.	r' -band(Cal.)	r' -band	z' -band(Cal.)	z' -band	y' -band(Cal.)	y' -band
–	(degree)	(degree)	(mag)	(error)	(mag)	(error)	(mag)	(error)
00003	7.5382657	−3.4150763	19.68	0.005	18.78	0.019	18.58	0.019
00005	7.5532112	−2.6132801	18.98	0.004	18.12	0.010	18.06	0.010
00007	7.5655923	−0.8315454	19.09	0.003	18.88	0.017	18.50	0.017
00010	7.5725584	−1.1528383	19.42	0.004	18.86	0.017	18.81	0.017
00012	7.5846310	−1.1274981	18.87	0.004	18.19	0.013	18.21	0.013
00014	7.5900631	−1.3554831	19.60	0.005	18.92	0.017	18.54	0.017
00017	7.6109405	−1.3498433	19.71	0.006	18.86	0.021	18.80	0.021
00018	7.6171780	−1.2596067	18.67	0.003	17.92	0.009	17.57	0.009
00019	7.6186543	−2.5213161	19.34	0.005	18.64	0.016	18.53	0.016
00020	7.6182194	−0.9157354	20.43	0.006	19.54	0.020	19.15	0.020
00021	7.6219807	−0.8942896	19.96	0.005	18.96	0.017	18.72	0.017
00022	7.6349025	−0.8483992	20.77	0.009	19.51	0.031	19.47	0.031
00027	7.6502290	−3.2748003	20.58	0.007	19.47	0.033	19.08	0.033
00032	7.6967616	−1.7589675	20.31	0.007	19.76	0.031	19.93	0.031
00034	7.6956468	−2.6042531	19.77	0.007	19.12	0.024	19.32	0.024
00036	7.7025204	−1.6794195	20.55	0.009	19.43	0.020	19.33	0.020
00037	7.7029967	−1.4917775	19.32	0.003	18.66	0.019	18.57	0.019
00039	7.7089334	−3.6373649	18.62	0.003	17.79	0.011	17.83	0.011

Notes. Column 1: ID number of merging galaxies. Column 2: RA in degrees (J2000). Column 3: Dec. in degree (J2000). Columns 4, 6, and 8: r' -, z' -, and y' -band magnitudes after calibration with SDSS data. Columns 5, 7, and 9: photometric uncertainties of r' -, z' -, and y' -band data.

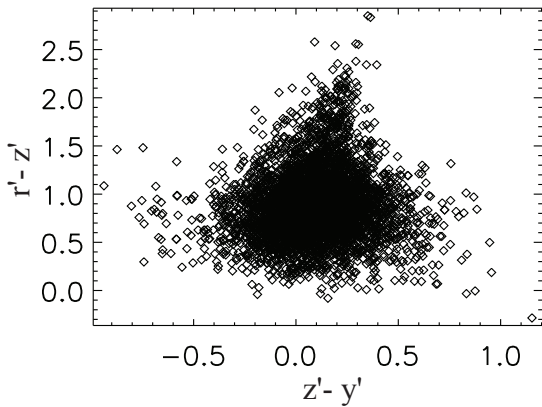


Fig. 2. Color–color diagram of the merging galaxies after calibrations with respect to SDSS. Mean uncertainties of $r' - z'$ and $z' - y'$ colors are 0.027 and 0.036, respectively.

3. Results

3.1. Preliminary classification and stellar mass

We classified our merging galaxies into three different types on the basis of the CFHT $g' - r'$ and $r' - z'$ colors. Firstly, we applied the homomorphic method to the CFHT images to get composite g' -, r' -, and z' -band photometry of merging systems. Secondly, we defined color regions of dry mergers, wet mergers, and mixed mergers on the basis of color evolutionary tracks with redshifts that are derived from galaxy templates (Fig. 3; see also Huang 2011; Coleman et al. 1980; Kinney et al. 1996). Mergers with composite colors in the elliptical region are classified as dry mergers, while mergers with combined colors in the starburst region are considered as wet mergers, and those objects with merged colors in the Sbc/Scd regions are regarded as mix mergers. It should be noted that our classifications are on the basis of blurred-together colors of both components of a merging system (e.g., luminosity-weighted combined colors), which

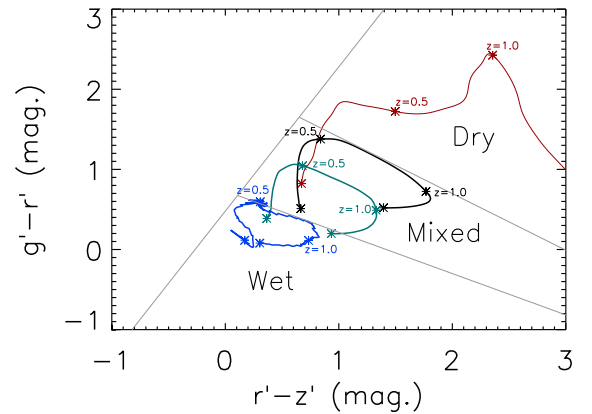


Fig. 3. Classification of mergers using composite CFHT colors. The tracks from top-right to bottom-left represent the colors of elliptical (red line), Sbc (dark line), Scd (green line), and starburst (blue line) galaxies at different redshifts. The boundaries of different classifications are showed in gray lines.

is different from the original definition of “gas-rich wet mergers” or “gas-poor dry mergers” (e.g., Lin et al. 2010). For comparison, we show an example of mergers of PS1 r' - and y' -band, CFHT r' -band, and SDSS r' -band in Fig. 4.

To derive the relation between the y' -band and stellar mass, we obtained the luminosities of the merging galaxies by using the spectral redshifts (spec- z) from the SDSS DR10 (Ahn et al. 2014). Approximately 200 merging galaxies in our sample have an available spec- z . We also obtained the $3.4 \mu\text{m}$ data of the merging galaxies from the Wide-Field Infrared Survey Explorer (WISE; Wright et al. 2010) archive to estimate stellar mass (Wen et al. 2013). Due to the poor resolution of the WISE $3.4 \mu\text{m}$ data ($6''$), we adapted photometry results directly from the WISE point source catalog instead of using the homomorphic-aperture method.

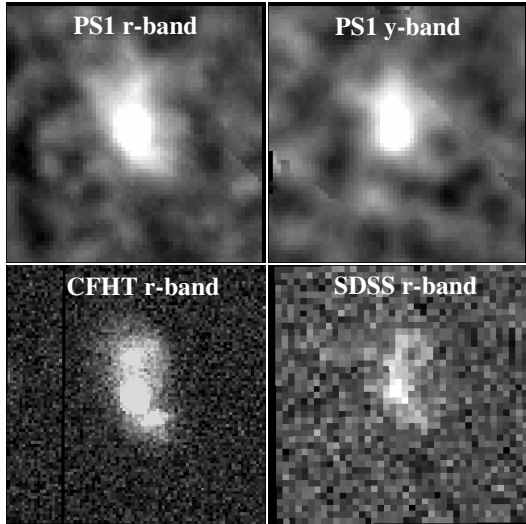


Fig. 4. Example of mergers of PS1, CFHT, and SDSS images. The size of each image is $\sim 15'' \times 15''$.

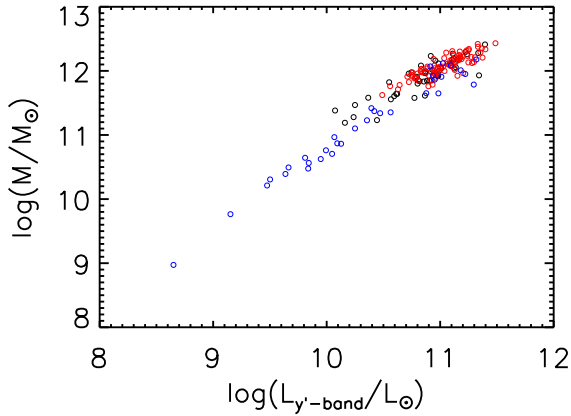


Fig. 5. Stellar mass derived from $3.4 \mu\text{m}$ - versus y' -band luminosities for different types of merging galaxies. Red: dry mergers; blue: wet mergers; black: mixed type.

To estimate the K -correction values, we adopted the elliptical, Sb/Sc, and starburst templates from Kinney et al. (1996) as the spectral energy distribution (SED) of the dry, mix, and wet mergers, respectively. The K -correction is defined as:

$$K(z) = 2.5 \log \left[(1+z) \frac{\int_0^{\infty} T(\lambda) S(\lambda) d\lambda}{\int_0^{\infty} T(\frac{\lambda}{1+z}) S(\lambda) d\lambda} \right], \quad (5)$$

where $T(\lambda)$ is the SED of the object and $S(\lambda)$ is the filter response function. Following the definition, we convolved the templates with the response function of the Pan-STARRS y' -band filter and the WISE $3.4 \mu\text{m}$ filter to obtain the K -correction value of each galaxy.

After performing the K -correction, we compared y' -band luminosity with the stellar mass derived from $3.4 \mu\text{m}$ luminosity for these merging galaxies (Fig. 5). The following equation represents the relation between the y' -band luminosity and the stellar mass for various color-merging galaxies. The equation can be written as

$$\log \left(\frac{M_*}{M_{\odot}} \right) = A \times \log \left(\frac{\nu L_{\nu}(y')}{L_{\odot}} \right) + B. \quad (6)$$

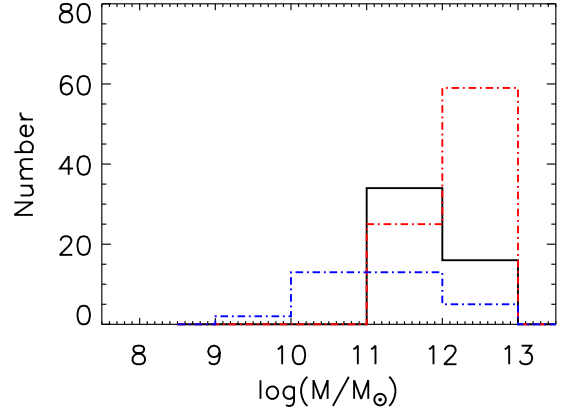


Fig. 6. Stellar mass distributions of the mergers with spec- z . Red: dry mergers; blue: wet mergers; black: mixed type.

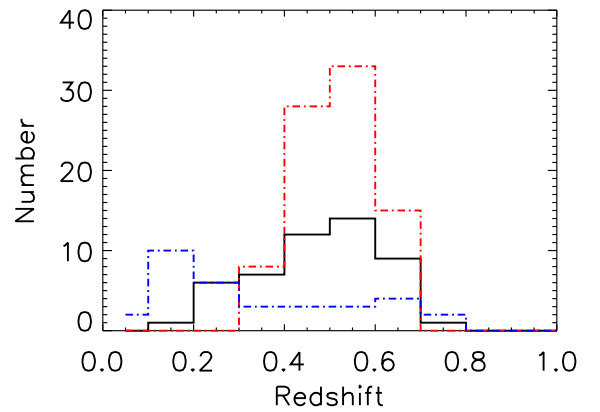


Fig. 7. Spectral redshift distributions for different types of mergers.

Here the parameter A denotes magnitude in y' -band luminosity, and the parameter B is color index of different types of merger: $A = 0.72$ and $B = 4.42$ for dry mergers; $A = 1.12$ and $B = -0.42$ for wet mergers; $A = 0.84$ and $B = 2.74$ for mix mergers.

Figures 6 and 7 provide the stellar mass and spec- z distribution of the mergers. The stellar mass of the dry mergers is between 10^{11} and $10^{13} M_{\odot}$, and that of the wet mergers is usually approximately $10^{11} M_{\odot}$ or less. In addition, the dry mergers distribute at higher redshifts than the wet mergers do (Fig. 7); the dry mergers distribute at redshifts of approximately 0.4–0.6, but most of the wet mergers distribute at redshifts of 0.2–0.3. Evidently, the stellar mass of the wet mergers is not as massive as that of the dry mergers. The luminosities of the wet mergers are usually weaker than those of the dry mergers; therefore, we could only detect the nearby wet mergers.

3.2. Stellar mass with photo- z

Because most of the mergers had no spec- z information, we estimated their luminosities by using the photometric redshift (photo- z) information. We first examined the relation between the spec- z and photo- z for 167 mergers with spec- z . We adopted the photo- z and spec- z data from SDSS DR10 (Ahn et al. 2014). Figure 8 shows the relation between the spec- z and photo- z for three different types of merging galaxies. We found that the photo- z data are strongly correlated with the spec- z data. This result indicated that we could use the photo- z to estimate the y' -band luminosity and to derive the stellar mass of the merging galaxies. We noted that uncertainties of photo- z for a particular

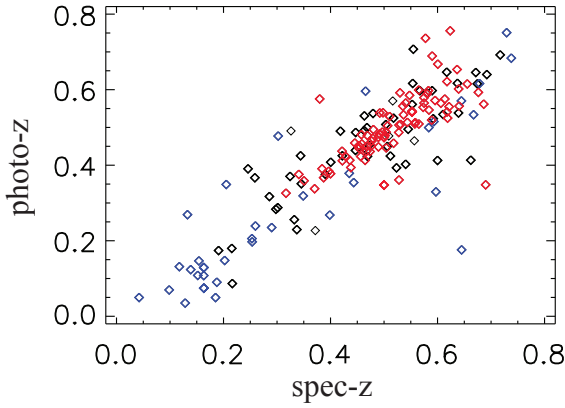


Fig. 8. Relation between photo- z data and spec- z data. Red diamonds: dry mergers; blue diamonds: wet mergers; black diamonds: mixed type.

source might be large; however, the distribution of the photo- z should represent the true redshift distribution of the sources in general, and the distributions of the physical quantities (e.g., luminosities) derived from the photo- z can thus provide useful information.

Approximately 3800 merging galaxies in our catalog had photo- z data. Figures 9 and 10 provide the results of the merging galaxies with photo- z . We determined that the distributions of the stellar mass were similar to the results derived using spec- z . The dry mergers were concentrated at approximately 10^{11} – $10^{12} M_{\odot}$, and the wet mergers peaked at $10^{10} M_{\odot}$. More wet mergers included photo- z , possibly because more faint wet mergers occurred, and these mergers are more difficult to observe using spectroscopy.

4. Discussion

We obtained the PS1 photometric results of merging galaxies by using adaptive apertures. The PS1 also provided photometric results in the Desktop Virtual Observatory (DVO). The DVO is a database that stores the observed results from PS1; the data in the DVO are derived after photometric and astrometric calibration. Because the results of the DVO are considered well-established and are widely used by the PS1 community, comparing our results with those from the DVO is crucial.

We first determined the color of the merging galaxies from the DVO. To avoid the confusion caused by astrometric uncertainty, we only considered the sources that had no double identifications. A total of 2022 merging galaxies in our catalog with PS1 y' -, r' -, and z' -band photometric data were obtained from the DVO database. We plotted the color–color diagram of the DVO results, as illustrated in Fig. 11; the colors are highly scattered, suggesting that substantial errors might exist in the DVO data.

To investigate the possible origin of the errors in the DVO, we reprocessed the sources with extreme colors by using our homomorphic-aperture process for the PS1 y' -, r' -, and z' -band images. We applied our algorithm and reprocessed the sources with the following three color regions: $r' - z' < -1$; $z' - y' > 2$, $2 < r' - z' < 3$ and $0 < z' - y' < 0.5$ to obtain the new photometric results. Figure 11 displays the reprocessed results. The reprocessed results distribute near the central region of the color–color diagram without substantial scattering. This suggests that the DVO photometric data might not provide an accurate estimation for these extended sources. However, the sources

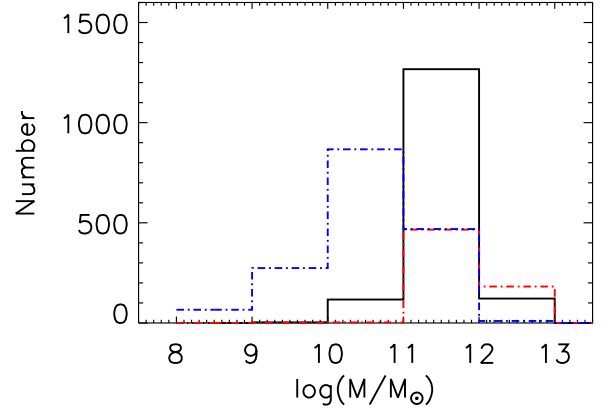


Fig. 9. Stellar mass distributions of the mergers with photo- z .

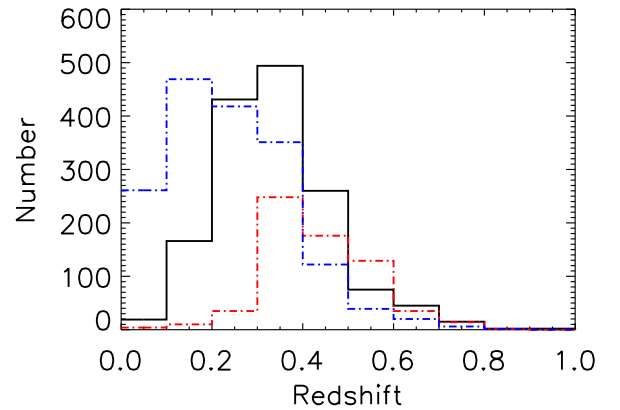


Fig. 10. Photometric redshift distributions for different types of mergers.

within the color region $2 < r' - z' < 3$ and $0 < z' - y' < 0.5$ maintained their original colors, indicating that the particular color distribution was not caused by data reduction errors. On the basis of the color–redshift relation of different types of galaxies derived from spectral templates (Coleman et al. 1980; Kinney et al. 1996), we concluded that the sources with the extreme color $2 < r' - z' < 3$ are likely to be distant giant elliptical galaxies (see Fig. 3).

We also compared the y' -band luminosities derived using our methods with the results of the DVO. Figures 12 and 13 provide comparison of the luminosity relations between the y' -band and the WISE 3.4 μm data of the DVO and our results for both dry and wet mergers. The linear relations between the y' -band and the WISE 3.4 μm data seem highly favorable for both the DVO and our results. However, the scatters of the DVO results are substantially larger than those of our results, suggesting that the uncertainty of the DVO measurements is considerably larger than that of our results. These merging galaxies are all extremely faint sources containing extended structures that are highly difficult to detect. Therefore, dedicated apertures and photometry are required. Processing these extended faint galaxies by using the automatic processes of the DVO package might be difficult. Our adaptive aperture method performed substantially more favorably than the DVO in measuring these extended faint sources.

Under the assumption that the 22 μm data of the WISE can be the star formation rate (SFR) indicator, we used the flux ratio of the 22 μm and y' -band data as the specific SFR (sSFR) indicator to compare the dry and wet mergers. Since some merging systems can be resolved as two galaxies at optical bands, the sSFR we estimated is a “luminosity-weighted” indicator.

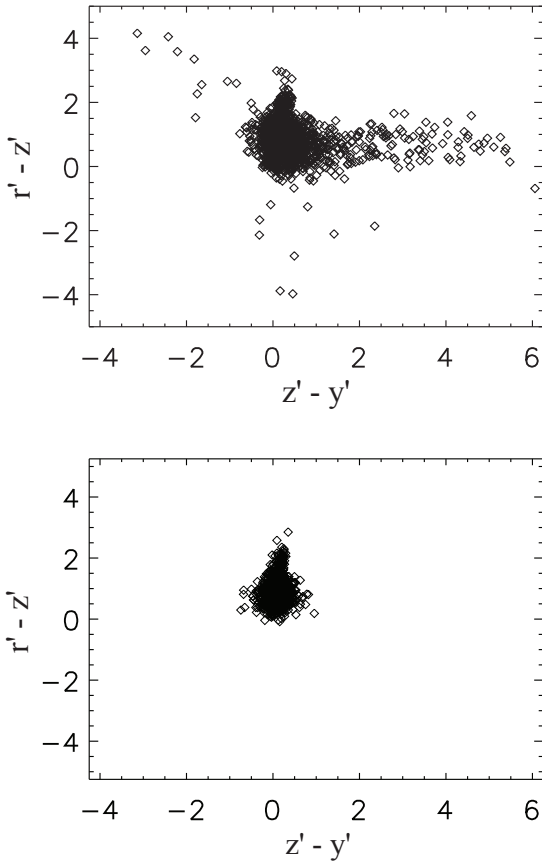


Fig. 11. *Upper:* color–color diagram of the merging galaxies obtained from the DVO data. *Bottom:* color–color diagram of the merging galaxies reprocessed with the homomorphic aperture method.

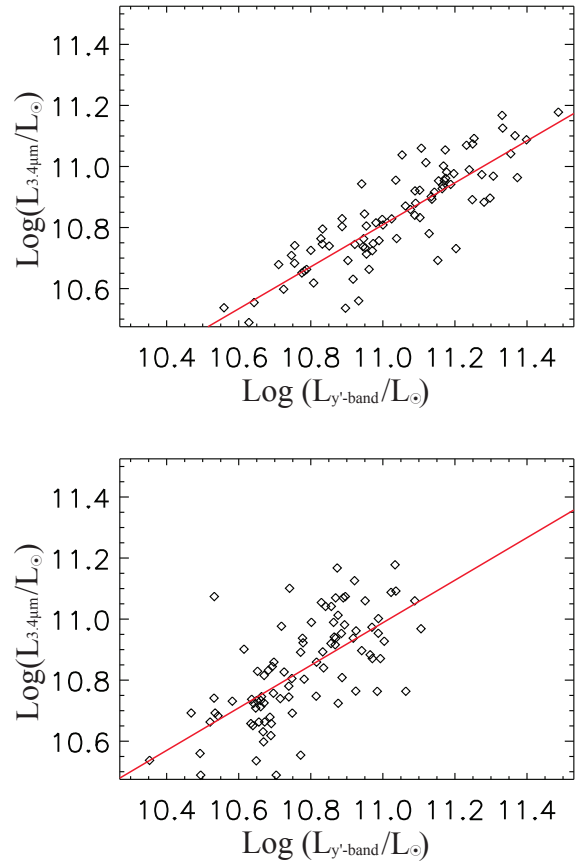


Fig. 12. Luminosity relations of the Pan-STARRS y' -band versus the WISE $3.4\ \mu\text{m}$ for the dry mergers. *Top:* the results from our homomorphic aperture method. *Bottom:* the results from the DVO data.

Figure 14 provides the sSFR of the dry and wet mergers; the distributions of the sSFR are similar between the dry and wet mergers. The dry mergers might have a high SFR because they are more massive ($10^{12} M_{\odot}$). We examined the spectra of these massive dry mergers; only four dry mergers have SDSS spectra. Most of these luminous “dry” mergers have signatures of star formation, such as [O II] $\lambda 3727$ emission line, and only one dry merger has a non-star-forming spectrum. We suggest that the dry mergers with star-formation signatures might be dusty star-forming galaxies.

Misclassification of merger types might be caused by overlaps between edges of different regions or dust reddening, and this will lead to uncertainties of photo- z . Firstly, the wet mergers with redshift >0.5 might be identified as the mix or dry mergers with redshift <0.5 . The effect can be clearly seen in Fig. 7; some outliers are located in the lower-right region with spec- $z >0.5$ and photo- $z <0.5$. Thus, $\sim 6\%$ (2/33) of the wet mergers, $\sim 10\%$ (5/50) of the mix mergers and $\sim 4\%$ (3/84) of the dry mergers with photo- $z <0.5$ might be originally the wet mergers with redshifts >0.5 . Secondly, the mix mergers with redshift >0.5 might be identified as the dry mergers with redshift >0.4 . The relation between spec- z and photo- z of the dry mergers are more scattered at higher redshifts, some outliers, for example, are located at spec- $z = 0.6$ and $0.6 < \text{photo-}z < 0.8$. Therefore, $\sim 6\%$ (5/84) of the dry mergers with $0.6 < \text{photo-}z < 0.8$ might be originally the mix merges at redshifts $z = 0.5\text{--}0.6$.

Bundy et al. (2005) and Naab et al. (2006) inferred that massive galaxies are formed by two or more merging processes in low redshift regions. However, according to our results, the dry

mergers usually occur at redshifts larger than 0.4, indicating that no dry mergers were detected in the nearby Universe. This might be due to selection effects: (1) as shown in Fig. 3, the dry mergers at redshifts less than 0.4 are misclassified as mix mergers; (2) Hwang & Chang (2009) set a size limit as a criterion when selecting the merging galaxies. They employed the size range from 20 to 100 pixels ($3.74''$ to $18.7''$) to select distant merging candidates. The fact that no nearby dry mergers were detected suggests that nearby dry mergers must be larger than the size limit and were excluded during the selection. By contrast, the wet mergers can be detected over the entire redshift range $0 < z < 0.7$; all the nearby mergers are wet mergers. The nearby wet mergers must be sufficiently small to be selected, but the distant wet mergers must be large enough to be detectable. These results suggest that small and large wet mergers exist, whereas only large dry mergers exist.

Bundy et al. (2005) demonstrated that the stellar masses of normal galaxies are approximately $10^{10}\text{--}10^{11} M_{\odot}$ in the $0.55 < z < 0.8$ region. This result is comparable with the stellar masses of the merging galaxies. Our results indicate that the stellar masses of the wet mergers also distribute near $10^{10}\text{--}10^{11} M_{\odot}$; by contrast, the stellar masses of the dry merging galaxies were concentrated at $10^{11}\text{--}10^{12} M_{\odot}$. Because the dry mergers processed several galaxy interactions, their masses are generally larger than those of the wet mergers. Our results illustrate that some of the dry mergers could be as massive as $10^{13} M_{\odot}$. Normal, elliptical and S0 galaxies, which might have encountered major mergers during their evolution, are usually more massive than spiral galaxies (Brinchmann & Ellis 2000). The mass distributions of

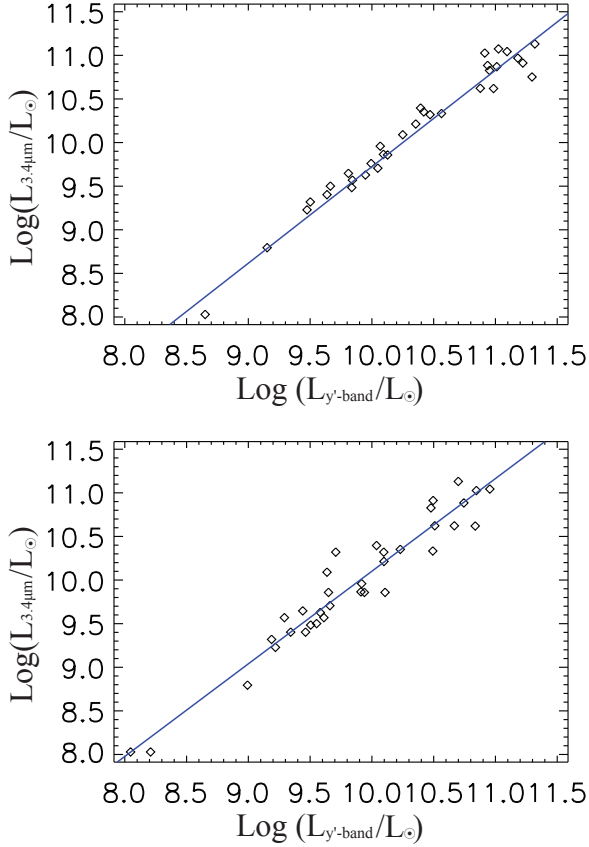


Fig. 13. Luminosity relations of the Pan-STARRS y' -band versus the WISE $3.4 \mu\text{m}$ for the wet mergers. *Top*: the results from our homomorphically-aperture method. *Bottom*: the results from the DVO data.

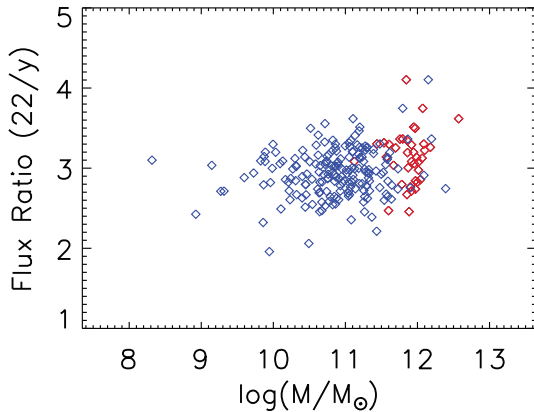


Fig. 14. sSFRs of the dry mergers and the wet mergers. We used the flux ratio of the WISE $22 \mu\text{m}$ to the Pan-STARRS y' -band emission as the sSFR indicator.

the dry and wet mergers are similar to those of elliptical and spiral galaxies, respectively.

5. Summary

We obtained the Pan-STARRS r' -, z' -, and y' -band photometric results of 4698 mergers by applying the homomorphically-aperture method, and estimated their stellar masses.

1. We set the detection threshold at 4σ and obtained the specific shapes of the merging galaxies for the photometric apertures.
2. We found that the homomorphically-aperture method can obtain more reasonable results than the DVO photometry can for some extended sources.
3. We discovered that the $3.4 \mu\text{m}$ luminosities of the WISE and the Pan-STARRS y' -band luminosities are well correlated. Because the $3.4 \mu\text{m}$ emission is a favorable indicator of the stellar mass of galaxies, we could use the y' -band results to estimate the stellar mass of galaxies.
4. We derived new relations between the Pan-STARRS y' -band luminosities and the stellar masses of the merging galaxies.
5. We found that the stellar masses of merging galaxies are approximately $10^{10} - 10^{12} M_{\odot}$; some of the dry mergers could be as massive as $10^{13} M_{\odot}$.

Acknowledgements. This work was partially supported by the Ministry of Science and Technology of Taiwan (grant MOST 103-2119-M-008-017-MY3). We thank L. H. Lin for useful comments and discussions. We also thank C. C. Lin, H. W. Lin, Y. T. Chen, J. K. Guo, I. C. Chen, & A. L. Tsai for helping this work. This discovery was enabled using the PS1 System operated by the PS1 Science Consortium (PS1SC) and its member institutions. The PS1 Surveys have been made possible through the combinations of the Institute for Astronomy at the University of Hawaii, The Pan-STARRS Project Office, the Max-Planck Society and its participating institutes, the Max Planck Institute for Astronomy, Heidelberg, and the Max Planck Institute for Extraterrestrial Physics, Garching, The Johns Hopkins University, the University of Durham, the University of Edinburgh, the Queen's University of Belfast, the Harvard-Smithsonian Center for Astrophysics, the Las Cumbres Observatory Global Network, and the National Central University of Taiwan. The PS1 Builders include: (alphabetically) W. S. Burgett, K. C. Chambers, T. Dombeck, T. Grav, J. N. Heasley, K. W. Hodapp, R. Jedicke, N. Kaiser, Rolf Kudritzki, Gerard Luppino, Robert H. Lupton, Eugene A. Magnier, David G. Monet, J. S. Morgan, P. M. Onaka, P. A. Price, P. H. Rhoads, Walter A. Siegmund, Christopher W. Stubbs, John L. Tonry, Richard J. Wainscoat, M. F. Waterson, and C. G. Wynn-Williams. This publication also makes use of data products from the Wide-field Infrared Survey Explorer, which is a joint project of the University of California, Los Angeles, and the Jet Propulsion Laboratory/California Institute of Technology, funded by the National Aeronautics and Space Administration. Funding for SDSS-III has been provided by the Alfred P. Sloan Foundation, the Participating Institutions, the National Science Foundation, and the US Department of Energy Office of Science. The SDSS-III web site is <http://www.sdss3.org/>. SDSS-III is managed by the Astrophysical Research Consortium for the Participating Institutions of the SDSS-III Collaboration including the University of Arizona, the Brazilian Participation Group, Brookhaven National Laboratory, Carnegie Mellon University, University of Florida, the French Participation Group, the German Participation Group, Harvard University, the Instituto de Astrofísica de Canarias, the Michigan State/Notre Dame/JINA Participation Group, Johns Hopkins University, Lawrence Berkeley National Laboratory, Max Planck Institute for Astrophysics, Max Planck Institute for Extraterrestrial Physics, New Mexico State University, New York University, Ohio State University, Pennsylvania State University, University of Portsmouth, Princeton University, the Spanish Participation Group, University of Tokyo, University of Utah, Vanderbilt University, University of Virginia, University of Washington, and Yale University.

References

- Ahn, C. P., Alexandroff, R., Allende Prieto, C., et al. 2012, *ApJS*, **203**, 21
Ahn, C. P., Alexandroff, R., Allende Prieto, C., et al. 2014, *ApJS*, **211**, 17
Brinchmann, J., & Ellis, R. S. 2000, *ApJ*, **536**, L77
Bundy, K., Ellis, R. S., & Conselice, C. J. 2005, *ApJ*, **625**, 621
Choi, C., Im, M., Jeon, Y., & Ibrahimov, M. 2012, *J. Korean Astron. Soc.*, **45**, 7
Cole, S., Lacey, C. G., Baugh, C. M., & Frenk, C. S. 2000, *MNRAS*, **319**, 168
Coleman, G. D., Wu, C.-C., & Weedman, D. W. 1980, *ApJS*, **43**, 393
Darg, D. W., Kaviraj, S., Lintott, C. J., et al. 2010, *MNRAS*, **401**, 1552
Davoodi, P., Pozzi, F., Oliver, S., et al. 2006, *MNRAS*, **371**, 1113
Ellison, S. L., Patton, D. R., Simard, L., & McConnell, A. W. 2008, *AJ*, **135**, 1877
Gilbank, D. G., Gladders, M. D., Yee, H. K. C., & Hsieh, B. C. 2011, *AJ*, **141**, 94

- Heijmans, H., & Ronse, C. 1990, *Comp. Vis. Graph. Im. Proc.*, **50**, 245
- Hodapp, K. W., Kaiser, N., Aussen, H., et al. 2004, *Astron. Nachr.*, **325**, 636
- Huang, J. C. 2011, Master Thesis, National Central Univ., Taiwan
- Huang, J. C., & Hwang, C.-Y. 2017, *PASP*, **129**, 034001
- Hwang, C.-Y., & Chang, M.-Y. 2009, *ApJS*, **181**, 233
- Kauffmann, G., Heckman, T. M., White, S. D. M., et al. 2003, *MNRAS*, **341**, 33
- Kinney, A. L., Calzetti, D., Bohlin, R. C., et al. 1996, *ApJ*, **467**, 38
- Lin, L., Koo, D. C., Weiner, B. J., et al. 2007, *ApJ*, **660**, L51
- Lin, L., Patton, D. R., Koo, D. C., et al. 2008, *ApJ*, **681**, 232
- Lin, L., Cooper, M. C., Jian, H.-Y., et al. 2010, *ApJ*, **718**, 1158
- Naab, T., Khochfar, S., & Burkert, A. 2006, *ApJ*, **636**, L81
- Nikolic, B., Cullen, H., & Alexander, P. 2004, *MNRAS*, **355**, 874
- Sheen, Y.-K., Yi, S. K., Ree, C. H., & Lee, J. 2012, *ApJS*, **202**, 8
- Tonry, J. L., Stubbs, C. W., Lykke, K. R., et al. 2012, *ApJ*, **750**, 99
- Toomre, A., & Toomre, J. 1972, *ApJ*, **178**, 623
- Tremonti, C. A., Heckman, T. M., Kauffmann, G., et al. 2004, *ApJ*, **613**, 898
- van Dokkum, P. G. 2005, *AJ*, **130**, 2647
- Wen, X.-Q., Wu, H., Zhu, Y.-N., et al. 2013, *MNRAS*, **433**, 2946
- Wright, E. L., Eisenhardt, P. R. M., Mainzer, A. K., et al. 2010, *AJ*, **140**, 1868
- Yee, H. K. C., Gladders, M. D., Gilbank, D. G., et al. 2007, in *Cosmic Frontiers*, eds. N. Metcalfe, & T. Shanks, *ASP Conf. Ser.*, **379**, 103
- York, D. G., Adelman, J., Anderson, Jr., J. E., et al. 2000, *AJ*, **120**, 1579